Ceramics International 47 (2021) 5523–5533

Contents lists available at ScienceDirect

Ceramics International

journal homepage: www.elsevier.com/locate/ceramint

Rational design of chemical bath deposition technique for successful preparation of Mn-doped CdS nanostructured thin films with controlled optical properties

Farzaneh Khani Kharabaneh [a], Elham Ghavidel [b], Ehsan Soheyli [c,*], Ahmet Faruk Yazici [d], Nawzad Nadhim Jawhar [e], Evren Mutlugun [f,**], Reza Sahraei [a,***]

[a] Department of Chemistry, Faculty of Science, Ilam University, 65315-516, Ilam, Iran
[b] Plasma Physics Research Center, Science and Research Branch, Islamic Azad University, Tehran, Iran
[c] Department of Physics, Faculty of Science, Ilam University, 65315-516, Ilam, Iran
[d] Department of Material Science and Nanotechnology Engineering, Abdullah Gul University, Kayseri, 38080, Turkey
[e] Department of Chemistry, College of Education, University of Garmian, 46021, Kalar, Iraq
[f] Department of Electrical-Electronics Engineering, Abdullah Gul University, Kayseri, 38080, Turkey

ARTICLE INFO

Keywords:
Thin films
Mn-doped CdS
Colloidal nucleation doping
Chemical bath deposition
Mn-related emission

ABSTRACT

The introduction of a rational design for depositing internally-doped nanostructured thin films is of great importance for optoelectronics. In this presented work, Mn-doped CdS thin films with high purity in composition were prepared through the chemical bath deposition technique using a nucleation-doping strategy. This work focuses on an improved chemical design to eliminate mostly ignored property of conventionally doped nanoscale thin films. The synthesis strategy was initiated by the initial formation of MnS nuclei in a colloidal depositing solution followed by injection of cadmium precursor to diffuse into the initial nuclei and play the role of host CdS matrix which was the beginning of the deposition process. Upon optimization of the PL-emission, it was revealed that relative intensity of Mn^{2+}-related peak to the excitonic peak has significantly increased (~100 times) in 80 °C, pH = 6, and precursor molar ratio of Cd:Mn:EDTA:S equal to 1:3:0.4:5, at deposition time of 300-min. The TRPL measurements further revealed the effective contribution of Mn-related midgap states with long-lived decay curve character, which confirms the success of the designed approach to reach internally doped thin films. It was found that the deposition temperature, amount of Cd/Mn/TA precursors, and deposition time are the most important experimental parameters in the proposed synthesis approach. Due to the versatility, generality, and colloidal advantages of this method, it can be extended to the other structures with various types of dopant agent.

1. Introduction

As one of the most applicable structures, nanostructured thin films with semiconducting electronic behavior are of utmost attention for fundamental researches with an industrial end [1]. Indeed, preparation of such structures is of particular importance for material science researchers and technologists in such a way that almost every sort of semiconductor compositions such as silicon, II-VI, I-III-VI_2, graphene, perovskites, and transition metal dichalcogenides has sparked the enthusiasm to prepare their corresponding thin films structures [2–7]. These films reveal engineered optical properties, which may not be possible using the bare synthesized forms of the nanocrystalline materials. Nonetheless, the long-time interest of scientists to enhance and control the physical properties of thin films has motivated them to focus on impurity doping strategies. Choosing the appropriate host matrix to involve dopant ions, a dopant ion to introduce/improve a specific characteristic, synthesis technique for deposition of nanocrystals (NCs), and finally, the synthesis-strategy are the key factors determining the quality of thin films.

II-VI semiconductor nanocrystals (NCs) are amongst the

* Corresponding author.
** Corresponding author.
*** Corresponding author.
E-mail addresses: ehs.soheyli@gmail.com (E. Soheyli), evren.mutlugun@agu.edu.tr (E. Mutlugun), r.sahraei@ilam.ac.ir (R. Sahraei).

https://doi.org/10.1016/j.ceramint.2020.10.136
Received 20 August 2020; Received in revised form 15 October 2020; Accepted 19 October 2020
Available online 20 October 2020

nanomaterials with relatively wide bandgap energy and accessible excitonic radius which have been used in the deposition processes [8] and can be effectively doped by desired impurity [9]. Cadmium sulfide is a semiconductor with a direct bandgap energy of 2.42 eV, which is of great importance for applications in LEDs, photocatalysts, and photodetectors [10–12]. They can be doped with a suitable amount of impurity to improve the photoelectronic/photovoltaic performance of the thin layers [13,14]. Jabeen et al. reported a better power conversion efficiency of about 0.4% for Mn:CdS NC thin films rather than CdS layers [15]. In another work, it has been demonstrated that using such structures as a buffer layer has a positive impact on the power conversion efficiency of Cu(In,Ga) $(S,Se)_2$-based solar cells with relatively high efficiency of about 15.8% [16]. Various deposition techniques have been employed to date to prepare CdS thin films doped with a particular dopant agent. Successive ionic layer adsorption and reaction (SILAR), chemical bath deposition (CBD), spray pyrolysis, electrodeposition, pulsed laser ablation, ion implantation, and spin-coating are some of the most utilized methods for deposition of the CdS based thin films [14, 16–21]. Since the beginning of doping nanocrystals with Bhargava and co-workers report in 1994 [22], the utmost attention has been dedicated to the manganese ions due to the parallel developments they add into the optical, electrical, and even magnetic properties of the host matrix. Particularly, it shows distinctive luminescent characteristics with a well-known emission peak at 580–590 nm.

The desired properties of a doped semiconductor can be achieved when additive ions are fit well into a host structure resolving the self-purification mechanism. However, the successful doping of the specific nanostructure with a dopant impurity is not an easy task and still needs to be studied due to the physicochemical limitations regarding the doping process [23]. In 2005, Pradhan et al. reported powerful methods based on the decoupling doping from nucleation and/or growth to prepare doped-semiconductor NCs in the colloidal phase [24]. Amongst them, the *nucleation-doping* strategy is quite successful to reach internally doped NCs in the colloidal approach [25]. It is performed by the initial formation of dopant-anion nuclei completed by the addition of the cation precursor of the host. Nonetheless, doping is much more difficult for nanostructured thin films. As has been overviewed in the literatures, it is clear that the details of the synthesis procedure are usually neglected in the researches performed in doped thin films deposited by chemical approach. In most of these works, the host and dopant cations are introduced together to the depositing solution [16, 26–30]. This method suffers from the low possibility of localization of dopant ions in the lattice structure as well as the remaining of less-controllable surface-adsorbed ions, which reduce the doping yield because of the small fraction of the added impurities are incorporated into the crystal lattice [31].

In the present work, we have considered a fundamental physicochemical aspect of how one can prepare real doped thin films. Since the most powerful technique for doping semiconductor NCs is the colloidal (reflux) method, we have employed the CBD technique, which is the most similar deposition technique to the colloidal methods with simplicity and upscaling capability. In more detail, the nucleation-doping strategy (which is utilized at the colloidal phase) is extended to the CBD technique to attain doped NCs in thin-film form. Although previous reports have focused on the simple co-presence of the dopant ions and main metal ions at the vicinity of substrates, in this present work, for the first time in the literature, we demonstrate the formation of Mn-doped CdS thin films via a chemical design. It was performed by the initial formation of dopant-anion nuclei followed by adding the host cations, offering a niche solution to control, and fine-tune the dopant amount and their optical properties. Besides, one can expect to reach better control over the electrical properties of doped thin films fabricated via this approach. This work considers a very important, mostly neglected, issue regarding the doping of nanostructured thin films, which can extend into other chemical deposition approaches, other types of host materials, and dopant ions as well.

2. Materials and types of equipment used

2.1. The materials used

$MnCl_2{\cdot}2H_2O$ (Merck), $Cd(CH_3COO)_2{\cdot}2H_2O$ (Merck), Thioacetamide: C_2H_5NS (Merck), EDTA: $C_{10}H_{14}N_2Na_2O_8{\cdot}2H_2O$ (Merck), and NaOH (Merck). Deionized water was used for the preparation of the deposition solution.

2.2. Preparation of Mn-doped CdS thin films

Mn-doped CdS thin films were deposited on commercial microscope slide glasses, which have no chemical reaction with the reaction solution during the coating process. The substrates were first cleaned by water. Then, they were immersed in sulphochromic acid solution for 24 h and rinsed with deionized water before transferring to the oven to dry at 50 °C. The chemical solution was prepared as follows: 12 mL of a 0.5 mol L^{-1} (M) Manganese chloride and 6 mL of a 0.2 M EDTA were dissolved in 20 mL of deionized water. The pH of the solution was initially 1.9 but adjusted to the desired values (4–7) by dropwise addition of 1 M NaOH. Next, 15 mL of a 1 M thioacetamide (TA) was added to the solution that has led to a gradual increase of pH. The solution was poured into a glass tank contained vertically placed glassy slides. Then, it was transferred to a thermostat bath set at a specific temperature. After 60 min of starting the reaction, when MnS species formed at the neighboring of substrates, 30 mL of a 0.1 M cadmium acetate was uniformly injected in situ with a syringe into the deposition solution. Upon injection of Cd precursor, the color of the solution immediately turned yellow and the deposition process was started. At different time intervals after the injection of Cd (120, 180, 240, 360, 480, 600 min), the glass slides were pulled out from the reaction tank and washed with deionized water. Then, it was stored in the slide holder to dry at room temperature. The initial molar ratio of precursors was Cd:Mn:EDTA:TA = 1:2:0.4:0.5. Various experimental parameters are involved during the deposition process and optimizing each of them can be considered to reach better nanostructured thin films with reproducible results. Therefore, the effect of changing initial experimental conditions on the optical properties of Mn-doped CdS thin films was investigated, including time and temperature of deposition process, pH, and precursor molar ratio of Cd:Mn:EDTA:TA.

2.3. Characterization techniques

Deposited thin films were characterized by Fourier-transform infrared spectroscopy (FTIR), X-ray diffraction (XRD), Energy Dispersive X-Ray Spectroscopy (EDX), and Field emission scanning electron microscopy (FE-SEM). The light absorbance properties of the as-deposited films were measured by Cary 300 Bio UV–Vis spectrophotometer (VARIAN) at the wavelength range of 300–800 nm. The PL emission spectra of nanoparticles were recorded using a Cary Eclipse fluorescence spectrophotometer (Agilent technology). The time-resolved PL measurements were performed by PicoQuant Fluo Time 200 time-correlated single-photon counting system equipped with a laser excitation source operating at 375 nm having a 5 MHz repetition rate. Lifetimes of the samples were collected with Time Harp 260 PICO system. The decay curves were modeled and amplitude average lifetimes were calculated by fitting the data with three exponentials using FluoFit software by PicoQuant Technologies. The X-ray photoelectron spectrum (XPS) of the prepared sample was performed via Thermo Scientific K Alpha X-Ray Spectrometer.

3. Results and discussion

Numerous efforts have been devoted to study doping of nanostructured thin films, yet in most of them doping agents and host matrix precursors were present in the reaction medium at the same time, and

the deposition process was performed in presence of both or even after preparation of host matrix. This leads to a weak surface-adsorbed doping with uncontrolled/non-reproducible physicochemical effects, as well as reduced dopant efficiency [32]. However, in this study, Mn and TA (as the source of sulfide) were first added to the depositing solution. It was carried out in the presence of EDTA to control the growth rate of MnS nuclei and prevent their possible fast precipitation. The solubility product constant (K_{sp}) of MnS is at the order of 10^{-13} [26]. Thus, by adding a suitable amount of Cd precursor, deposition follows a similar process to which used for nucleation-doping strategy in colloidal preparation of doped NCs [24]. Since, the K_{sp} value of CdS ($\sim 10^{-28}$) [33] is much lower than that of MnS, cadmium ions can contribute more effectively to the lattice structure of initial nuclei and play a role of host matrix for Mn ions. After the addition of cadmium, the color of the depositing solution changed to yellow, somehow confirming the formation of CdS NCs. By further continuation of the thermal process, thin layers of Mn-doped CdS NCs were deposited onto the substrates. This method is a powerful approach with excellent results in the colloidal-phase synthesis of NCs. However, to the best of our knowledge has not been used for nanostructured thin films so far.

3.1. Effect of Temperature

Deposition temperature is one of the most vital factors governing the quality and growth of nanostructured thin films. More importantly, it might be a determinative factor to reach a mostly internally doped nanostructure deposited on the substrate. In this work, the deposition of Mn-doped CdS thin film was performed at different temperatures of 40, 60, and 80 °C. Fig. 1 shows XRD patterns of deposited thin films on glass substrates at deposition temperatures of 60 and 80 °C. The XRD patterns of the bulk wurtzite CdS and MnS have been shown at the bottom of the XRD profile [34]. As can be observed, the XRD patterns contain broad peaks that are located near hexagonal (wurtzite) CdS, implying successful doping of Mn in the structure of thin films [35]. Besides, the intensity of the pattern increases slightly with raising the temperature from 60 to 80 °C, somehow indicating the growth of nanoparticles' size. Indeed, based on the well-known Scherer equation, the size of nanocrystallites increased from 5.35 nm for a deposition temperature of 60 °C to 5.53 nm for 80 °C.

FE-SEM images of Mn-doped CdS thin films deposited on glass substrates at different deposition temperatures are shown in Fig. 1B. As can be seen, the layers deposited at 40 °C have pores and are heterogeneous, but as the deposition temperature increases, thin films become more homogeneous and the film deposited at 80 °C is almost without pores. It is also clear that the particles approximate a spherical shape. In addition, as deposition temperature increases, Mn-doped CdS particles grow in good agreement with the results of X-ray diffraction.

Fig. 1C illustrates the absorption spectra of Mn-doped CdS thin films deposited in various temperatures, at Mn:Cd = 2 M ratio. With the rising temperature, the absorption of thin films has increased at all wavelengths, which is due to the thickness-increase of the films. On the other hand, the radius of NCs increased by raising the temperature, making a red-shift in the wavelength of absorption edge from approximately 460 to 489 nm that is found to be in good agreement with the observed trend in SEM images.

The fundamental absorption, which corresponds to electron excitation from the valence band to the conduction band, can be used to calculate bandgap energy (E_g). Bandgap energy is determined from the absorption coefficient using the Tauc relation:

$$\alpha h\upsilon = k\left(h\upsilon - E_g\right)^m \quad (1)$$

where α is the absorption coefficient, h is the Planck constant, ν is incident photon frequency, k is a constant which is related to the effective masses associated with the valence and conduction bands, and m is a value depending on the nature of the transition. It is a constant equal to *1/2* for direct allowed transition and *2* for the indirect allowed transition. In this regard, the E_g of thin films can be calculated by plotting $(\alpha h\upsilon)^2$ versus $h\upsilon$ and extrapolating the straight-line portion of the curve to zero absorption coefficients ($\alpha = 0$). With raising the temperature from 40 to 80 °C, the energy gap of samples decreases from 2.7 to 2.54 eV, which is quite closer to the bandgap energy of bulk CdS (2.42 eV). This is a direct consequence of the quantum confinement effect discovered by the Brus equation, indicating that a decrease in the size of semiconductor NCs is associated with an increase in bandgap energy vice versa. This also implies that the weak quantum confinement regime

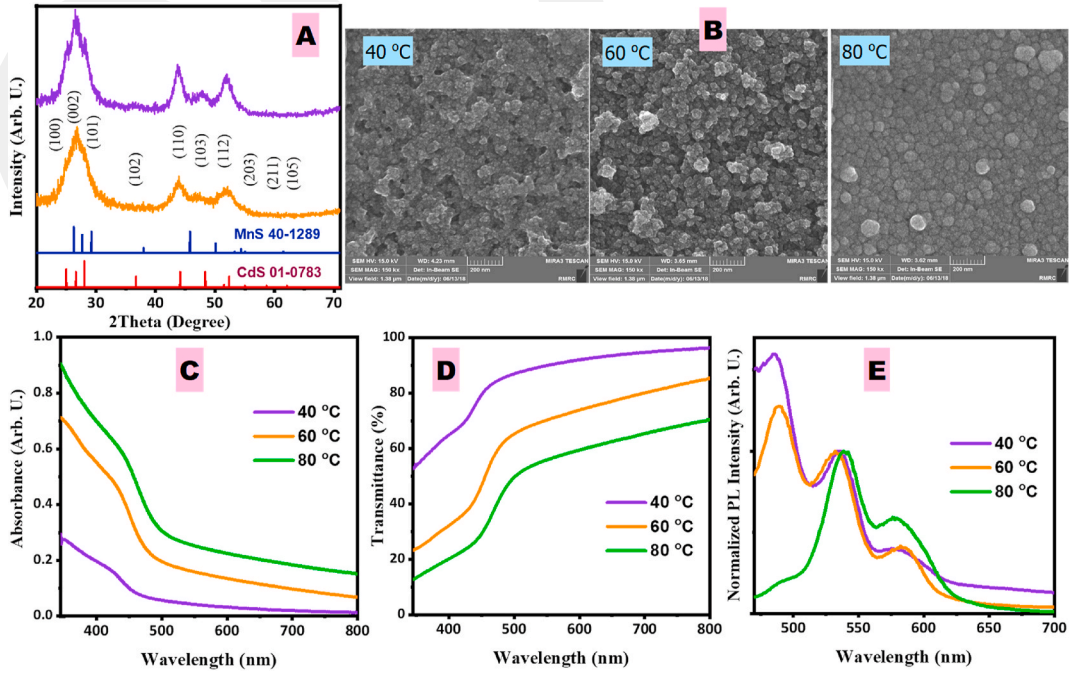

Fig. 1. (A) XRD patterns, (B) FE-SEM images (at the magnification-scale of 200 nm), (C) UV–Vis absorption spectra, (D) Transmittance spectra, and (E) Normalized PL spectra of Mn-doped CdS thin films deposited on glass substrates at 40, 60 and 80 °C. The molar ratio of the precursors was Cd:Mn:EDTA:TA = 1:2:0.4:0.5.

is dominant for the present system. This conclusion was made based on the size of nanoparticles, which exceeds the exciton Bohr radius for CdS (R_{ex} = 5.8) [36]. Furthermore, the absorption edge wavelength of the prepared sample is near that of the bulk hexagonal CdS structure (512 nm).

The transmission spectra of as-deposited Mn-doped CdS thin films also confirmed the results of absorption spectra. As can be seen in Fig. 1D, the highest transmittance occurred at 40 °C, where it is more than 85% at the visible region of wavelengths and the lowest transmittance occurred at 80 °C, where its value is typically 50–60%. An obvious shift in the absorption edge towards longer wavelengths was also detected with deposition temperature. This redshift and decline of transmittance intensity indicate an increase in the size of the nanoparticles as well as an increase in the thickness of thin films, respectively. Shape and position of transmittance spectra are similar to those reported for CBD-deposited Sn:CdS thin films [37].

In addition to the results of XRD and FE-SEM analyses, the size of the semiconductor nanoparticles can be estimated using the results of the UV–Vis–NIR spectrum. In this work, three different well-known methods are used for this purpose.

Effective mass approximation: In this case, the approximate particle size is calculated based on the framework of Brus's equation:

$$E_n - E_b = \left(\frac{h^2}{8R^2}\right)\left(\frac{1}{m_e^*}+\frac{1}{m_h^*}\right) - 1.8\frac{e^2}{\varepsilon R} \quad (2)$$

where e is an elementary charge of the electron (1.602×10^{-19} coulombs), ϵ is dielectric constant (5.7 for CdS), h is Planck constant (4.13567×10^{-15} eV S), E_n and E_b are the optical bandgap energies of CdS nanoparticles and the corresponding bulk state, R is the radius of grains (assuming that the nanoparticles are almost spherical), m_e* and m_h* are effective masses of electron and hole, respectively; equal to 0.21 m_0 and 0.8 m_0 in CdS ($m_0 = 9.1 \times 10^{-31}$ kg is the electron rest mass). By taking into account these values, the following relation is obtained:

$$E_n - E_b = \left(\frac{14.1}{R^2}\right) - \left(0.065 \times \frac{10^{-38}}{R}\right) \quad (3)$$

Regardless of the second term on the right side of Eq. (3), which is related to Coulomb interaction, we then have:

$$D_1 = 2R = 2 \times \left[\left(\frac{14.1}{E_n - E_b}\right)\right]^{\frac{1}{2}} \quad (4)$$

Empirical relations: Two different formulas have been suggested for this model [38].

$$D_2 = \frac{0.1}{0.1338 - 0.0002345\lambda_a} \quad (5)$$

$$D_3 = \left(-6.65 \times 10^{-8}\right)\lambda_a^3 + \left(1.95 \times 10^{-4}\right)\lambda_a^2 - \left(9.23 \times 10^{-2}\right)\lambda_a + 13.29 \quad (6)$$

where λ_a is the wavelength of the absorption edge. The crystallites size of the deposited nanostructures prepared at different temperatures are presented in Table 1. Regardless of the method used to calculate, the crystallites size increases with rising temperature, and the optical bandgap declines at the same time, which confirms the results obtained from FE-SEM and XRD. However, there is a clear difference in the values estimated by effective mass approximation with the others. This is attributed to the different approximations considered in each approach [39]. The present results are quite similar to those reported by Rodríguez et al., for Sn-doped CdS thin-films grown by light-assisted chemical bath deposition process [40].

Table 1
Crystallites size estimation of Mn-doped CdS thin films prepared at different deposition temperatures.

	Temperature of deposition (°C)	40	60	80
	Optical bandgap (eV)	2.7	2.58	2.54
Crystallites Size (nm)	Effective mass approximation (D_1)	14.2	18.7	21.68
	Empirical formula (D_2)	3.86	4.71	5.23
	Empirical formula (D_3)	5.72	6.66	7.12

Fig. 1E shows the normalized PL spectra of Mn-doped CdS thin films deposited at pH~6, the molar ratio of Cd:Mn:EDTA:TA = 1:2:0.4:0.5, and different temperatures. The PL spectra recorded at room temperature and the excitation wavelength of 430 nm consist of three main peaks. Excitonic states can be involved in the emission process by recombination of excited electrons and remained holes in the valence band. This process leads to an emission peak of around 490 nm. The possibility of recombination through impurities and structural defects is the reason for intense PL emission at around 530 nm as well as those observed at longer wavelengths [19]. The spectra also exhibit an emission at about 585 nm, due to the recombination of carriers through mid-gap energy levels of Mn^{2+} [41]. It is worth mentioning that these levels can play the role of deep trap-states localized within the bandgap region. To clarify the variation of PL emission spectra in a more pronounced way, all the results were normalized for the middle peak. Because the nature of the recombination processes through midgap-energy levels are somehow similar while they are quite different from band-to-band/excitonic recombinations.

At the depositing temperature of 40 °C, the emission related to the Mn^{2+} dopant ions/deep trap-energy levels has the lowest intensity. This can be illustrated based on the reaction sequence described above; at the first stage, the small nuclei of MnS cores were prepared, followed by injection of Cd for preparation of Mn:CdS NCs. Probably at 40 °C, the crystalline quality of NCs is not high enough, making the lattice full of defect-sites. Furthermore, the high K_{sp} value of Mn–S along with the lack of suitable thermal condition results in a depositing solution with a low density of MnS nuclei. Therefore, upon the injection of cadmium, there is not a required amount of manganese to play the role of dopant ions within the CdS host matrixes. This means that the excitonic emission is the prominent one. On the other hand, the peak located at ~585 nm grows as temperature increases from 40 to 60 °C and it becomes intense when the temperature reaches 80 °C, while the excitonic peak drops significantly. These observations further support our assertion. Indeed, by raising deposition temperature to 80 °C, Mn^{2+} ions have a better condition to take part in the formation of initial MnS nuclei in the depositing solution. This provides CdS NCs with higher levels of internally incorporated Mn dopant ions. Hence, as can be seen in the PL spectrum of thin films prepared at 80 °C, the excitonic emission has decreased drastically while dopant-related emission enhances. Here, the 80 °C was selected as the optimal temperature for continuing the reaction.

To understand the nature of the recombination process in the structure, for the 80 °C deposited nanostructured thin films, we have performed time-resolved spectroscopy measurements (Fig. 2A). The peaks at 490, 530, and 585 nm have been set at the emission monochromator end of the system, revealing the emission dynamics from the corresponding band levels. The photoluminescence decays have been fit with three exponentials, also indicating the nonradiative paths observed from the analysis. The peak at the 490 nm, which corresponds to bandgap emission, reveals an amplitude average lifetime of 0.511 ns, with 3-lifetime components of 0.996, 0.105, and 5.887 ns. The long-lived lifetime component is attributed to the main radiative recombination sites, whereas the fast lifetime components correspond to nonradiative recombination, which hinders the high photoluminescence characteristics of the samples under consideration. The long-lived τ_3 component is the maximum (7.49 ns) for the 585 nm peak, corresponding to the midgap energy levels of Mn ions. Therefore, various radiative and non-radiative energy centers are contributed to the recombination process making the TRPL profile a multiexponential decay curve. On the other hand, it reveals that the Mn ions introduced their energy levels within the bandgap region based on the long-lived

Table 2
The atomic percentage of elements in Mn-doped CdS nanocrystalline thin films prepared with different nominal Mn:Cd molar ratios obtained from EDX analysis.

Mn:Cd nominal molar ratio		0	0.4	1	1.2	2	3	4
The atomic percentage of elements (EDX)	S	49.64	49.32	48.99	48.11	47.79	48.83	50.22
	Mn	0	0.18	0.35	0.51	0.62	1.07	1.05
	Cd	50.36	50.50	50.67	51.38	51.59	50.10	48.73
Cd:S real molar ratio		1.01	1.02	1.03	1.07	1.08	1.03	0.97
Mn:Cd real molar ratio		0	0.004	0.007	0.010	0.013	0.021	0.022

component for 585 nm peak. This further supports the success of the suggested method for effective doping of Mn ions into the CdS host matrix. The details of the TRPL fitting results have been included in the Supporting Information (Table S1).

The surface electronic structures and chemical compositions (at the 5–10 nm thickness surface layer) of Mn-doped CdS thin films were evaluated by XPS measurement (Fig. 2B–E). The measurement was performed twice before and after etching, but the XPS profile was the same in both cases. Two characteristic bands at about 405 and 412 eV are related to the Cd $3d_{5/2}$ and Cd $3d_{3/2}$, respectively. Overlapped peaks with binding energies of ~161 and 163 eV are due to the S $2p_{3/2}$ and S $2p_{5/2}$, respectively. Besides, a weak XPS peak centered near 653 eV can be related to the Mn $2p_{3/2}$. These results demonstrate the presence of the main components of the thin film structures (Cd, and S) including the lower amounts of Mn^{2+} ions as dopant agents. The XPS data also reveals a weak surface oxygen-related peak that could propose some oxidation effects at the surface of nanostructures. Such observations have been reported elsewhere [15,42,43]. The obtained data indicate that all the expected elements are notably present at the lattice of the deposited nanostructures. Specifically, the presence of Mn-related peak demonstrates the ability of the present method to deposit a real Mn-doped CdS NCs.

The FT-IR spectrum of a typical thin film deposited at 80 °C for 300 min, and pH value of 6 in the range of 400–4000 cm^{-1}, has revealed two weak absorption bands at about 1600 and 3420 cm^{-1} which are attributed to H–*O*–H bending and stretching vibrations, confirming the presence of small amounts of water (Fig. S1). It rejects the presence of organic compounds or unwanted impurities such as cadmium oxide (CdO) or cadmium hydroxide ($Cd(OH)_2$) in the structure of deposited layers.

3.2. Effect of solution pH

To study the effect of pH on optical properties of Mn-doped CdS thin films, the pH of the depositing solution was adjusted to ~4, 5, 6, and 7 before the injection of TA. The absorption spectra of Mn-doped CdS thin films deposited at different pH values are shown in Fig. 3A. It was found that the absorption intensity of thin films is almost independent of changing the pH of the solution. The lowest absorbance of Mn-doped CdS thin films occurs at pH = 6–7 and the highest at pH of 4. Meanwhile, the absorption edge has shifted slightly towards longer wavelengths with an increase in the value of pH.

The transmission spectra of the thin films are shown in Fig. 3B. The transmittance recorded for pH = 4 was the lowest one, confirming the results of absorption spectra.

The normalized PL spectra of Mn-doped CdS thin films deposited at 80 °C, for 300 min, the molar ratio of Mn:Cd = 2, and at different pH values are shown in Fig. 3C. The optimized pH value was 5–6, where the impurity's/deep levels' emission is more intense, and the peak corresponding to the excitonic state decreases considerably. However, the solution pH of 6 was used for subsequent syntheses.

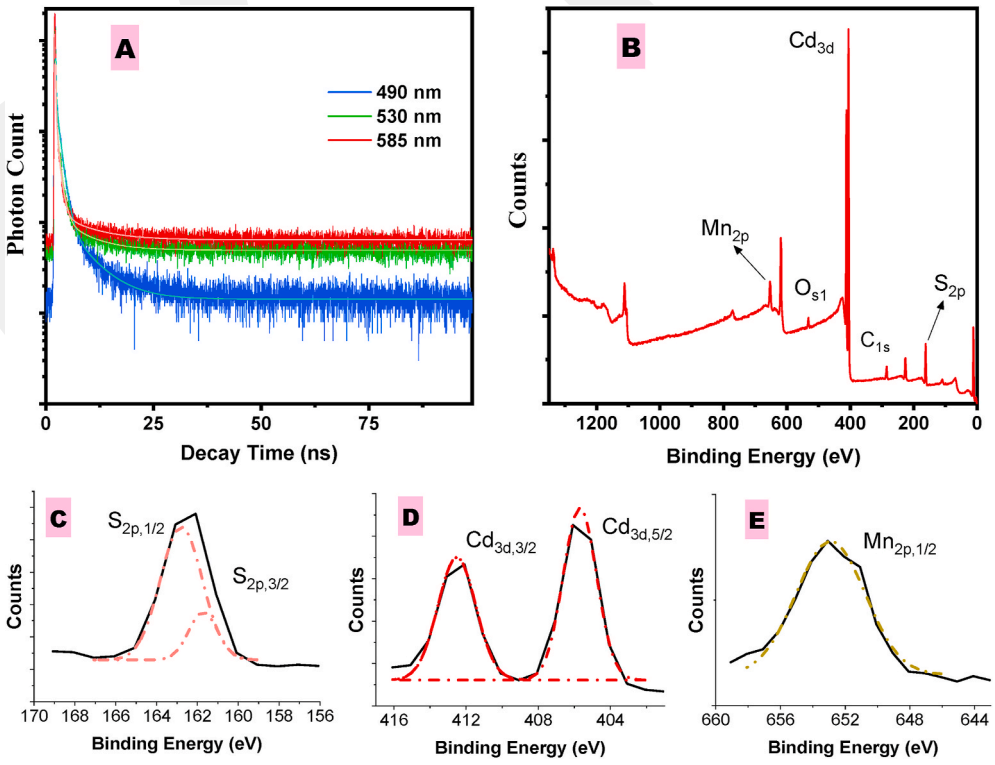

Fig. 2. (A) Time-resolved PL (corresponding to peak emissions from the steady-state photoluminescence measurements), and (B–E) XPS measurements of the Mn:CdS sample prepared at 80 °C with Mn:Cd molar ratio of 3.

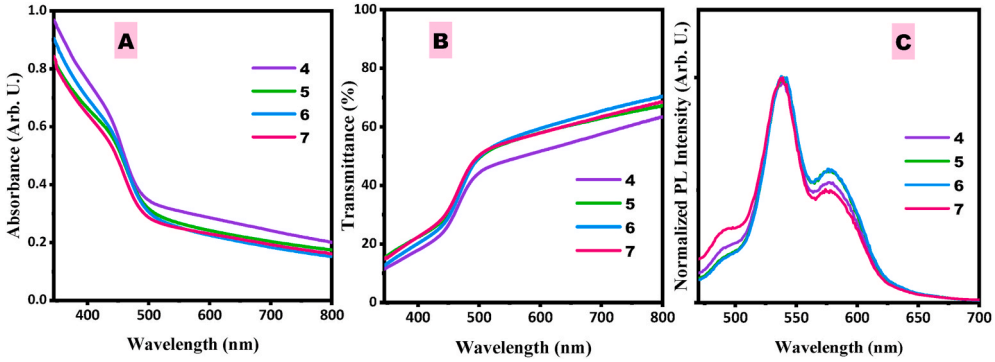

Fig. 3. (A) UV–Vis absorption spectra, (B) Transmittance spectra, and (C) Normalized PL spectra of Mn-doped CdS thin films deposited at different solution pH. The precursors molar ratio was Cd:Mn:EDTA:TA = 1:2:0.4:0.5 and the depositing temperature was 80 °C.

3.3. Effect of precursor molar ratio

Change in amount of EDTA: As mentioned previously, the deposition procedure began with the formation of MnS nuclei in the depositing solution. Hence, for depositing Mn-doped CdS NCs on glassy substrates, the initial solution must be stable enough and prevent the agglomeration of MnS nuclei. In this regard, the presence of a required amount of EDTA is mandatory to achieve the desired result. EDTA molecules can bind to Mn^{2+} and then Cd^{2+} ions to form Mn-EDTA/Cd-EDTA complexes and control the deposition rate.

Different amounts of EDTA were used (0.75, 1, 1.2, 1.5, and 3 mmol) for changing the Cd:EDTA molar ratios to 1:0.25, 1:0.33, 1:0.4, 1:0.5, 1:1 (or 4, 3, 2.5, 2, and 1, respectively). As shown in Fig. 4A, the absorbance of Mn-doped CdS thin films is in the highest value for Cd:EDTA molar ratio of 4, and with an increase in EDTA amount to 3, the spectra shifts to lower intensities. This supports the idea of EDTA's influence on the deposition rate. The thinner layer of Mn-doped CdS NCs forms at high concentrations of EDTA and the thicker layer at lower concentrations. However, there is no meaningful change in absorption intensity with a further decrease in Cd:EDTA molar ratio from 3 to 1, indicating that it is no longer effective on the deposition rate of NCs. The absorption edge also shows a similar trend and with a decrease in Cd:EDTA molar ratio from 4 to 3, it shifts to longer wavelengths, and then it is approximately independent on the amount of EDTA.

Fig. 4B shows the transmission spectra of Mn-doped CdS thin films prepared in different Cd:EDTA molar ratios. As expected from the absorption results, the lowest transmittance is obtained at Cd:EDTA = 4, and the spectra are almost similar for other ratios.

The normalized PL spectra of Mn-doped CdS thin films deposited at 80 °C for 300 min, at different Cd:EDTA molar ratios are shown in Fig. 4C. As can be seen, the intense PL emission of impurity/deep levels, as well as the considerable reduction in emission of excitonic states, have occurred when the molar ratio of Cd:EDTA was 2.5 (or equivalently 1:0.4).

Change in amount of cadmium: To evaluate the effect of Cd concentration on optical properties of Mn-doped CdS thin films, different amounts of Cd were used (0.3, 3, and 15 mmol). In this regard, the corresponding molar ratios of Cd:EDTA were 12.5, 2.5, and 0.25. Fig. 5A shows the absorption spectra of Mn-doped CdS thin films prepared with different concentrations of Cd. As can be observed, minimum and maximum absorbance values have been reported for 0.3 and 15 mmol of Cd. The absorption intensity for 0.3 mmol of cadmium is very low and approximately approaches zero at wavelengths longer than 550 nm. On the other hand, upon the injection of the higher amounts of Cd in the second phase of the deposition process, the formation possibility of CdS species is enhanced. Therefore, the growth rate and thickness of films increases which in turn raises the absorbance. Also, with increasing Cd concentration, the absorption edge shifts to shorter wavelengths, from 515 to 490 nm. As shown in Fig. 5B, the highest and lowest transmittance values are obtained in the solutions that contained 0.3 and 15 mmol of Cd, respectively.

Fig. 5C illustrates the room temperature PL spectra of Mn-doped CdS thin films deposited with different concentrations of Cd. In small amounts of cadmium ions, the peak related to recombination through Mn energy levels is very weak. The formation of CdS host nuclei is limited by the concentration of Cd ions in the depositing solution. The presence of a small amount of Cd at the second phase of the deposition process along with the low capability of Mn ions to form MnS species results in these observations in the PL emission spectrum. With an increase in the amount of cadmium precursor to 3 mmol (30 mL of 0.1 M cadmium acetate), the excitonic emission drops significantly, while emission peak related to the Mn^{2+}/deep-trap levels intensifies. It can be

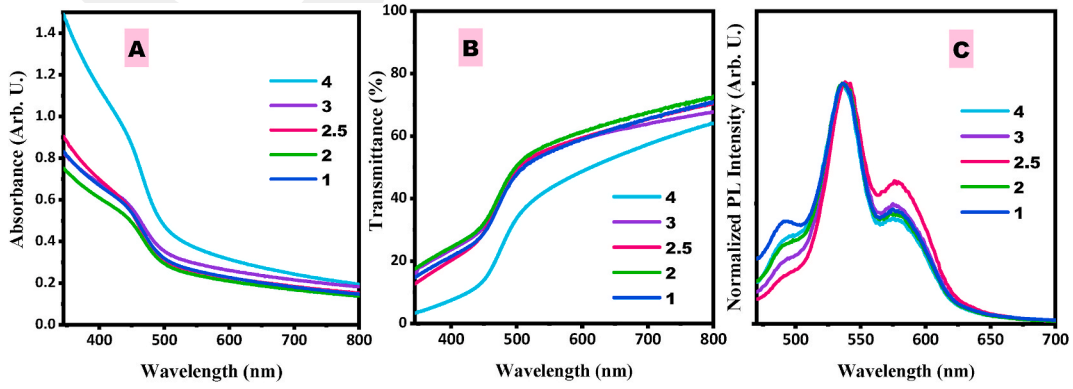

Fig. 4. (A) UV–Vis absorption spectra, (B) Transmittance spectra, and (C) Normalized PL spectra of Mn-doped CdS thin films deposited at different Cd:EDTA molar ratios. The precursors molar ratio was Cd:Mn:TA = 1:2:0.5 and the depositing temperature was 80 °C.

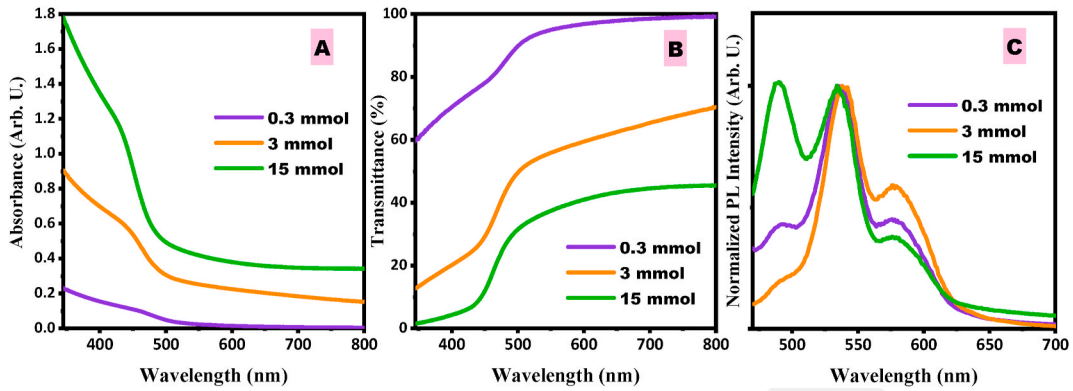

Fig. 5. (A) UV–Vis absorption spectra, (B) Transmittance spectra, and (C) Normalized PL spectra of Mn-doped CdS thin films deposited at different amounts of Cd. The precursors molar ratio was Mn:EDTA:TA = 2:0.4:0.5 and the depositing temperature was 80 °C.

attributed to better Mn-doping within the CdS host matrix. Meaningfully, with further increase in Cd amount, the strong enhancement in excitonic-related PL emission intensity along with the reduction of the longer-wavelength peak is observed. This confirms that at an elevated level of Cd^{2+} ions, the possibility for the formation of CdS nuclei increases, enhancing the excitonic PL emission. Results for the present nucleation-doping method showed that 3 mmol of Cd (when the molar ratio of Cd:Mn was equal to 1:2) led to optimum PL emission with better Mn^{2+}/deep-trap emission at long wavelengths.

Change in amount of Mn: The present work focuses on the demonstration of a powerful and developed doping strategy in thin film deposition. Therefore, optimization of the required dopant amount for optical properties sounds to be necessary. Different concentrations of Mn precursor (0, 1.2, 3, 3.6, 6, 9, and 12 mmol in accordance with molar ratios of Mn:Cd = 0, 0.4, 1, 1.2, 2, 3, 4, respectively) were used for as-deposited Mn-doped CdS thin films. Three X-ray diffraction patterns at different molar ratios of Mn:Cd equal to 0.4, 1, and 3 have been shown in Fig. 6. As can be seen, increasing Mn concentration does not affect the number of peaks, as well as their locations and the type of crystalline structure. The multi-peak nature of the patterns as revealed at the inset of Fig. 6A implies that deposited Mn-doped CdS nanostructures were crystallized in a hexagonal lattice structure. The average size of the NCs was also estimated using the Debye–Scherrer formula showed growth with the increase in Mn content (5.53, 5.78, 5.94 nm).

To date, most of the publications on doped thin films have reported that particle size decreases with increasing dopant concentration [28,32,44–46]. However, the average size estimated in this work shows growth in the size of particles that can be attributed to the differences in the chemical method used between those reported by others and the present method. As illustrated above, the present method started with the formation of MnS nuclei at the depositing solution, and with an increase in Mn content, the initial nuclei might be formed with a larger size. It somehow decouples the doping and growth processes.

Fig. 6 demonstrates the typical EDX spectrum of Mn-doped CdS thin films at Mn:Cd of 0.4, 1.2, and 3 all the original EDX profiles have been provided in Fig. S2 of supporting information). The quantitative results

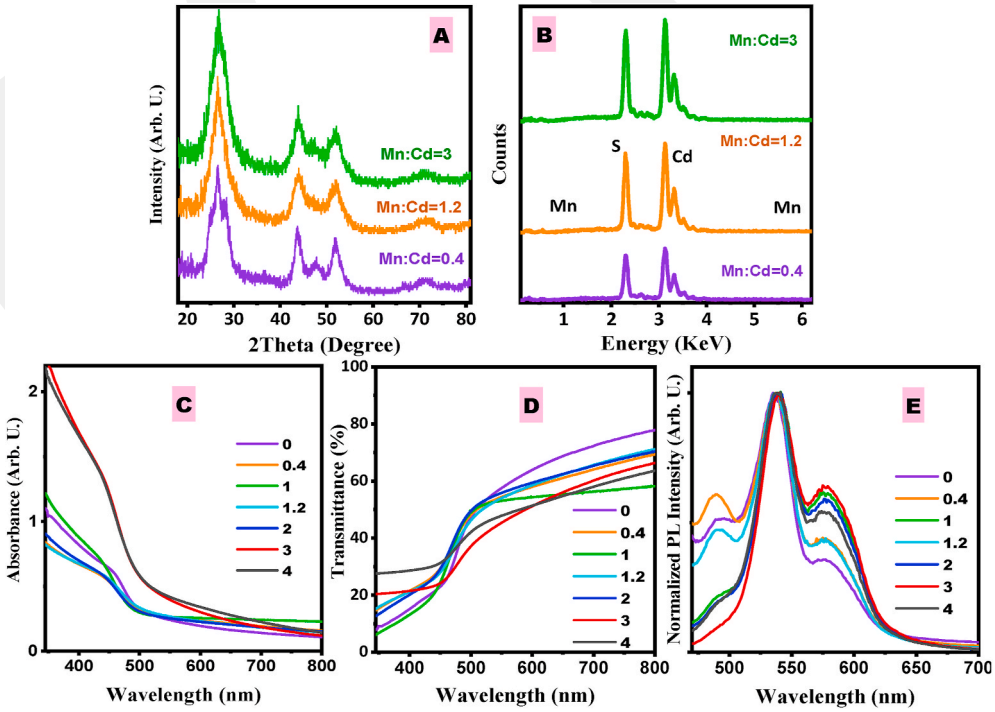

Fig. 6. (A) XRD patterns, (B) EDX profiles, (C) UV–Vis absorption spectra, (D) Transmittance spectra, and (E) Normalized PL spectra of Mn-doped CdS thin films deposited on glass substrates at different molar ratios of Mn:Cd, deposition temperature of 80 °C for 300 min. The precursors molar ratio was Cd:EDTA:TA = 1:0.4:0.5.

summarized in Table 2, showing interesting results. For the nanostructured thin films deposited at different Mn amounts, the ratio of Cd:S is quite near 1 which confirms the formation of the CdS matrix in a well-stoichiometric condition.

On the other hand, as the concentration of Mn^{2+} ions used during the deposition process increases (from Mn:Cd = 0 to 4), its real percentage localized in the CdS nanostructure is also raised (from Mn:Cd = 0 to 0.021). This huge difference between the nominal and real amounts of dopant concentration is a convenient observation in such nanostructures, which further demonstrates the difficulties encounter with the doping process. Besides, Table 2 shows that with an increase in the concentration of Mn (from Mn:Cd = 2 to 4), the proportion of Cd to S has decreased, indicating the substitution of Mn for Cd in the structure of thin film-constituent NCs. It should be noted that by increasing the concentration of Mn in the precursor solution, the solubility product constant (K_{sp}) decreases that leads to the formation of a higher level of initial Mn–S nuclei. Thus, at higher concentrations, higher amounts of Mn ions can be localized as internal impurities with greater amounts in the host matrix. Table 2 clearly illustrates that the highest amount of Mn dopant agents was in the molar ratio of Mn:Cd = 3 with 1.07%, and it decreased to 1.05 when the molar ratio of Mn:Cd was 4.

As Fig. 6C shows, the absorption spectra of Mn-doped CdS thin films prepared at various Mn-to-Cd molar ratios have a trivial non-linear characteristic for both of absorption edge and absorption intensity. Trivial effect on intensity factor of spectra somehow indicates that low concentration of Mn does not lead to a meaningful effect on the thickness of thin films and there is no meaningful deposition before the addition of Cd precursor. Nevertheless, at the high concentrations of Mn precursor the absorption intensity increases which can be attributed to increasing the thickness of deposited layers. The transmission spectra of thin films are provided in Fig. 6D, confirming the result of absorption spectra prepared at different molar ratios of Mn:Cd.

Successful localization of dopant ions is accompanied by profound changes in the physicochemical properties of the host matrix. One of these aspects is their emission behavior in the presence of dopant ions. Localized dopant ions act as a new recombination site for the excited electron-hole pairs, resulting in altered luminescence properties of the host matrix. The room temperature PL spectra of Mn-doped CdS thin films prepared at different Mn:Cd molar ratios are showed in Fig. 6E. The peak at 585 nm can correspond to Mn impurities (from the first excited state $^4T_1$ to the ground level $^6A_1$) [26] and deep-trap sites. As the Mn^{2+} dopant ratio increases, the intensity of peak at 585 nm rises while excitonic emission almost disappears. It can be seen that the most intense emission assigned to Mn^{2+} belongs to the Mn:Cd = 3 molar ratio which contains the highest real amount of Mn in EDX analysis. However, as the concentration of Mn^{2+} further increases (from Mn:Cd = 3 to 4), the density of dopant ions and their corresponding energy levels increase, resulting in a higher level of energy transfer between the sites of the dopant levels. In this case, the extra energy of the excited carriers transfers between these energy levels, and the radiation will no longer be emitted. An excessive increase in the density of dopant ions results in non-irradiated levels, which reduces the intensity of PL emission. These results strongly suggest that Mn^{2+} ions are successfully substituted in the host matrix. The best emission results were obtained for the Mn:Cd molar ratio of 3.

Change in the amount of TA: The presence of a suitable amount of anions is of great importance to reach high-quality semiconductor nanostructures, and this is more important when someone looking for a doped one. In this regard, to investigate the effect of TA concentration on optical properties of Mn-doped CdS thin films, different amounts of TA were used (0.75, 1.5, 6, 15, 21, 27 mmol) which changed molar ratios of Cd:TA to 4, 2, 0.5, 0.2, 0.14, 0.11. However, the molar ratios of Cd:Mn:EDTA were remained constant at 1:3:0.4. The thin films were prepared at 80 °C and the solution pH of 6.

As Fig. 7 shows, the highest and lowest absorbance occurs at Cd:TA = 0.2 and 4, respectively. At the lowest concentration of TA, the concentration of anion sites to form Cd–S structures is low leading to the formation of thin layers of nanostructures on the substrates. However, by a gradual increase in TA concentration to Cd:TA = 0.2, the rate of deposition grows. With further increase in TA amount, the undesired density of anion sites makes an opposite trend in the growth of nanostructures resulting in a drop in the absorbance intensity. As can be seen, a completely similar trend occurred for transmittance spectra (Fig. 7B). Mn-doped CdS thin films deposited at a molar ratio of Cd:TA = 4 has the highest transmittance (around 90% at longer wavelengths), while Cd:TA = 0.2 shows the lowest transmittance, (about 50%).

Fig. 7C shows the great influence of TA concentration on normalized PL emission characteristics of Mn-doped CdS thin films. As it demonstrates, in small doses of TA (Cd:TA = 4), the relative intensity of doping agents' emission is very low compared to other peaks while excitonic and shallow-defect emissions are dominant, probably due to sulfur vacancies. It can be illustrated as follows. Since the K_{sp} of CdS (1×10^{-28}) is much lower than that of MnS (3×10^{-13}), at a fixed amount of materials, CdS is more likely to form, and at low amounts of TA, there are insufficient anionic sites to form MnS structure. No doping likely to take place. However, with raising TA concentration, there is a significant increase (more than 20 times) in the relative intensity of doping agents' emission in comparison to other emissions because of the growth in the density of required anionic sites for Mn dopant ions. The optimum PL emission has been obtained at 15 mL of 1 M TA (equal to Cd:TA = 0.2). Beyond the optimal amount of TA, with raising the concentration of TA, the proportion of Cd to TA decreases, and in turn the intensity of doping agents' emission declines. An excessive concentration of anions can increase the likelihood of non-radiative recombination of charge carriers [47]. Besides, there is a 10 nm red shift in the PL emission peak related to shallow defect-traps with increasing the TA amount, which can be attributed to the change in density/energy of midgap sulfur-sites.

3.4. Change in deposition time

The time of deposition is one of the factors governing significant effects on the physical properties of thin films. The time effect was studied at 180, 240, 300, 420, 540, 660 min after the start of the reaction (the time duration of the first step was fixed at 60 min). Fig. 8 displays the FE-SEM images of Mn-doped CdS thin films deposited at 80 °C, pH = 6, at different deposition times of 180, 300, and 540 min. It is apparent from the micrographs that all films have good adherence to their substrates. The average grain size increases with increasing deposition time, ranging from 20 nm to 80 nm.

Fig. 8 Shows the absorption spectra of Mn-doped CdS thin films prepared at different times of deposition. As can be seen, the highest absorbance occurs at 300 min of deposition. On the contrary, the lowest absorbance is obtained at 660 min. It somehow reveals that upon the initial increase in the deposition time, the thickness of the layers on the glass substrates increases as well. Nonetheless, at longer deposition times, above 300 min, not only deposition does not occur but also the increase in structural strain causes destruction of layers and reducing the thickness of layers. On the other hand, there is no noticeable change in the absorption edge with increasing deposition time.

Transmission spectra of the thin films prepared at different times of deposition are shown in Fig. 8C. The lowest transmittance has been obtained at 300 min and the highest occurred at 660 min, as expected.

The normalized PL spectra of Mn-doped CdS thin films deposited at different times of deposition are demonstrated in Fig. 8D. With increasing time duration of deposition, the peak at around 580 nm has raised which is attributed to the doped Mn^{2+} ions in the host structure of CdS. The peak reaches its highest intensity when the deposition time is equal to 300 min, but it has dropped in longer times. It can be stated that with an initial increase of deposition time, the probability of a more efficient substitution of Mn^{2+} in the host structure of CdS increases. However, as the deposition time was raised to more than 300 min, the thickness of layers has increased and the increasing possibility of the

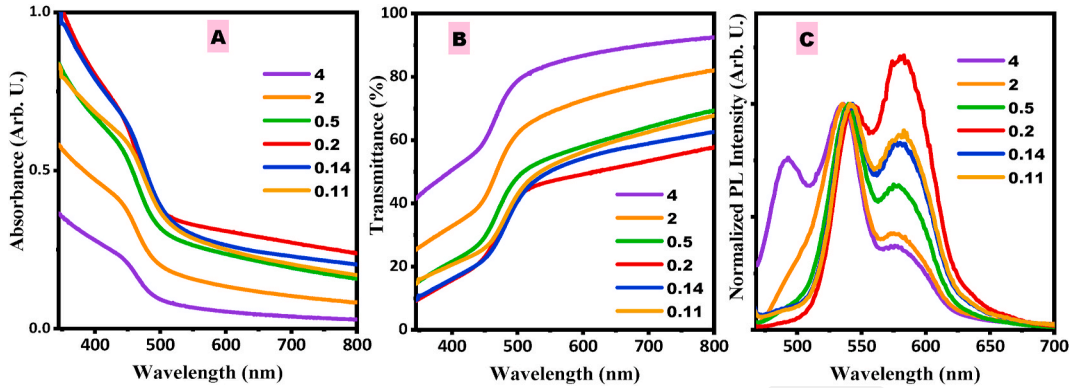

Fig. 7. (A) UV–Vis absorption spectra, (B) Transmittance spectra, and (C) Normalized PL spectra of Mn-doped CdS thin films deposited at different molar ratios of Cd to TA. The precursors molar ratio was Cd:Mn:EDTA = 1:3:0.4 and the depositing temperature was 80 °C.

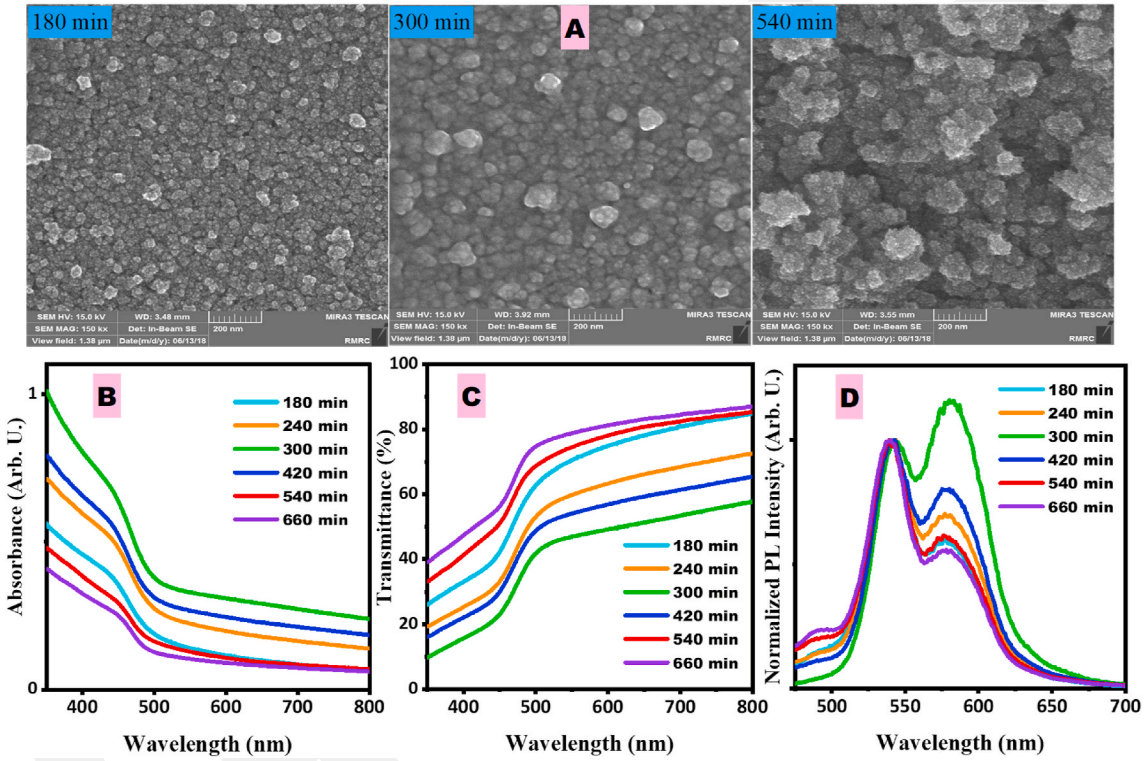

Fig. 8. (A) FE-SEM images (at the magnification-scale of 200 nm), (B) UV–Vis absorption spectra, and (C) Transmittance spectra and (D) Normalized PL spectra of Mn-doped CdS thin films deposited on glass substrates at different deposition times. The precursors molar ratio was Cd:Mn:EDTA:TA = 1:3:0.4:5.

formation of lattice mismatches has led to the elevated intra-structural strain and thereby raising the density of structural defects.

4. Conclusion

Inspired by the powerful nucleation-doping strategy in colloidal synthesis of semiconductor NCs, here we developed it to the CBD technique for fabricating Mn-doped CdS thin film NCs. Considering the advantages of the large difference in solubility products of Mn–S and Cd–S, initial nuclei of MnS were formed in the presence of EDTA (at the deposition solution). Then a suitable amount of Cd precursor was added to effectively diffuses into the MnS nuclei and form CdS host NCs containing small amounts of Mn^{2+} ions as dopant species. This step was followed by the deposition of yellow layers containing Mn:CdS NCs on the glass substrates. Structural analysis revealed that a well-deposited nanoscale CdS lattice with small amounts of Mn dopant ions have been prepared with a stoichiometric character and hexagonal phase polycrystalline nature. A set of experimental optimizations were performed on the synthesis procedure to make thin-film characters reproducible with optimized PL emission results. The special attention was paid to enhance the well-known ~580 nm emission peak of Mn energy levels. The TRPL measurements confirmed the co-presence of non-radiative/radiative recombination centers as well as long-lived emission through Mn energy levels. It was found that the deposition temperature, amount of Cd/Mn/TA precursors, and deposition time are the most important experimental parameters in the proposed synthesis approach. The simplicity of the designed strategy, as well as the excellent results regarding structural and optical properties of Mn-doped CdS thin films, demonstrate the merits of the suggested method for internal doping of the host matrix in thin-film form. On the other hand, due to the versatility and generality of this method, it can be used for the deposition of other structures with various types of dopant agent.

CRediT authorship contribution statement

Farzaneh Khani Kharabaneh: Investigation, Formal analysis, Visualization. **Elham Ghavidel:** Validation, Writing - original draft. **Ehsan Soheyli:** Conceptualization, Formal analysis, Methodology, Validation, Visualization, Writing - original draft, Writing - review & editing. **Ahmet Faruk Yazici:** Investigation, Formal analysis, Data curation. **Nawzad Nadhim Jawhar:** Investigation, Formal analysis. **Evren Mutlugun:** Resources, Validation, Methodology, Writing - review & editing. **Reza Sahraei:** Project administration, Conceptualization, Funding acquisition, Resources, Validation, Writing - review & editing.

Declaration of competing interest

The authors declare that they have no known competing financial interests or personal relationships that could have appeared to influence the work reported in this paper.

Appendix A. Supplementary data

Supplementary data to this article can be found online at https://doi.org/10.1016/j.ceramint.2020.10.136.

References

[1] S.M. Pawar, B.S. Pawar, J.H. Kim, O.S. Joo, C.D. Lokhande, Recent status of chemical bath deposited metal chalcogenide and metal oxide thin films, Curr. Appl. Phys. 11 (2011) 117–161, https://doi.org/10.1016/j.cap.2010.07.007.

[2] M. Zhang, H. Lin, S. Deng, R. Chen, G. Li, S.T. Han, Y. Zhou, Y. Yan, W. Zhou, M. Wong, H.S. Kwok, High-performance polycrystalline silicon thin-film transistors without source/drain doping by utilizing anisotropic conductivity of bridged-grain lines, Adv. Electron. Mater. 6 (2020) 1900961, https://doi.org/10.1002/aelm.201900961.

[3] K. Ou, L. Bai, M. Huang, L. Yi, X. Duan, S. Wang, Effect of preparation parameters on deep-blue light-emitting diodes based on nanostructured ZnSe/ZnS multilayer films, ACS Omega 5 (2020) 24567–24573, https://doi.org/10.1021/acsomega.0c03071.

[4] T. Adhikari, D. Pathak, T. Wagner, R. Jambor, U. Jabeen, M. Aamir, J.M. Nunzi, Structural, optical, electrochemical and photovoltaic studies of spider web-like Silver Indium Diselenide Quantum dots synthesized by ligand mediated colloidal sol-gel approach, Opt. Mater. 73 (2017) 70–76, https://doi.org/10.1016/j.optmat.2017.08.005.

[5] G. Bae, D.S. Song, Y.R. Lim, I. Jeon, M. Jang, Y. Yoon, C. Jeon, W. Song, S. Myung, S.S. Lee, C.-Y. Park, K.-S. An, Chemical patterning of graphene via metal-assisted highly energetic electrons irradiation for graphene homojunction-based gas sensors, ACS Appl. Mater. Interfaces (2020), https://doi.org/10.1021/acsami.0c12063.

[6] S. Shao, H. Duim, Q. Wang, B. Xu, J. Dong, S. Adjokatse, G.R. Blake, L. Protesescu, G. Portale, J. Hou, M. Saba, M.A. Loi, Tuning the energetic landscape of ruddlesden-popper perovskite films for efficient solar cells, ACS Energy Lett 5 (2020) 39–46, https://doi.org/10.1021/acsenergylett.9b02397.

[7] C.Y. Chang, K.S. Anuratha, Y.H. Lin, Y. Xiao, P. Hasin, J.Y. Lin, Potential-reversal electrodeposited MoS_2 thin film as an efficient electrocatalytic material for bifacial dye-sensitized solar cells, Sol. Energy 206 (2020) 163–170, https://doi.org/10.1016/j.solener.2020.06.001.

[8] A.L. Rogach, N.A. Kotov, D.S. Koktysh, A.S. Susha, F. Caruso, II-VI semiconductor nanocrystals in thin films and colloidal crystals, Colloids Surfaces A Physicochem. Eng. Asp. 202 (2002) 135–144, https://doi.org/10.1016/S0927-7757(01)01072-X.

[9] R. Sahraei, S. Darafarin, Preparation of nanocrystalline Ni doped ZnS thin films by ammonia-free chemical bath deposition method and optical properties, J. Lumin. 149 (2014) 170–175, https://doi.org/10.1016/j.jlumin.2014.01.040.

[10] R. Grover, R. Srivastava, O. Rana, A.K. Srivastava, K.K. Maurya, K.N. Sood, D. S. Mehta, M.N. Kamalasanan, Electroluminescence from hybrid organicinorganic LEDs based on thermally evaporated CdS thin films, J. Lumin. 132 (2012) 330–336, https://doi.org/10.1016/j.jlumin.2011.08.021.

[11] H. Feng, N. Tang, S. Zhang, B. Liu, Q. Cai, Fabrication of layered (CdS-Mn/MoS_2/CdTe)-promoted TiO_2 nanotube arrays with superior photocatalytic properties, J. Colloid Interface Sci. 486 (2017) 58–66, https://doi.org/10.1016/j.jcis.2016.09.048.

[12] Y. Zhao, M. Yuan, Y. Chen, Y. Huang, J. Lian, S. Cao, H. Li, L. Wu, Size controllable preparation of sphere-based monolayer CdS thin films for white-light photodetectors, Ceram. Int. 44 (2018) 2407–2412, https://doi.org/10.1016/j.ceramint.2017.10.210.

[13] M.P.A. Muthalif, C.D. Sunesh, Y. Choe, Enhanced light absorption and charge recombination control in quantum dot sensitized solar cells using tin doped cadmium sulfide quantum dots, J. Colloid Interface Sci. 534 (2019) 291–300, https://doi.org/10.1016/j.jcis.2018.09.035.

[14] M. Shkir, I.M. Ashraf, S. AlFaify, A.M. El-Toni, M. Ahmed, A. Khan, A noticeable effect of Pr doping on key optoelectrical properties of CdS thin films prepared using spray pyrolysis technique for high-performance photodetector applications, Ceram. Int. 46 (2020) 4652–4663, https://doi.org/10.1016/j.ceramint.2019.10.196.

[15] U. Jabeen, T. Adhikari, D. Pathak, S.M. Shah, J.M. Nunzi, Structural, optical and photovoltaic properties of P3HT and Mn-doped CdS quantum dots based bulk hetrojunction hybrid layers, Opt. Mater. 78 (2018) 132–141, https://doi.org/10.1016/j.optmat.2018.02.019.

[16] T.-M. Cheng, C.-H. Cai, W.-C. Huang, W. Xu, L.-H. Tu, C.-H. Lai, Efficiency enhancement of Cu(In,Ga)(S,Se)$_2$ solar cells by indium-doped CdS buffer layers, ACS Appl. Mater. Interfaces 12 (2020) 18157–18164, https://doi.org/10.1021/acsami.0c02416.

[17] J. Kaza, M.R. Pasumarthi, P.S. Avadhani, Superstrate and substrate thin film configuration of CdS/CZTS solar cell fabricated using SILAR method, Optic Laser. Technol. (2020), https://doi.org/10.1016/j.optlastec.2020.106413.

[18] S.Z. Werta, O.K. Echendu, K.O. Egbo, F.B. Dejene, Electrochemical deposition and characterization of thin-film $Cd_{1-x}Zn_xS$ for solar cell application: the effect of cathodic deposition voltage, Thin Solid Films 689 (2019) 137511, https://doi.org/10.1016/j.tsf.2019.137511.

[19] G. Perna, V. Capozzi, M. Ambrico, V. Augelli, T. Ligonzo, A. Minafra, L. Schiavulli, M. Pallara, Structural and optical characterization of undoped and indium-doped CdS films grown by pulsed laser deposition, Thin Solid Films (2004) 453–454, https://doi.org/10.1016/j.tsf.2003.11.105.

[20] S. Chandramohan, A. Kanjilal, S.N. Sarangi, S. Majumder, R. Sathyamoorthy, T. Som, Implantation-assisted Co-doped CdS thin films: structural, optical, and vibrational properties, J. Appl. Phys. 106 (2009), 063506, https://doi.org/10.1063/1.3224867.

[21] T. Chtouki, Y. El Kouari, B. Kulyk, A. Louardi, A. Rmili, H. Erguig, B. Elidrissi, L. Soumahoro, B. Sahraoui, Spin-coated nickel doped cadmium sulfide thin films for third harmonic generation applications, J. Alloys Compd. 696 (2017) 1292–1297, https://doi.org/10.1016/j.jallcom.2016.12.089.

[22] R.N. Bhargava, D. Gallagher, X. Hong, A. Nurmikko, Optical properties of manganese-doped nanocrystals of ZnS, Phys. Rev. Lett. 72 (1994) 416–419, https://doi.org/10.1103/PhysRevLett.72.416.

[23] S.C. Erwin, L. Zu, M.I. Haftel, A.L. Efros, T.A. Kennedy, D.J. Norris, Doping semiconductor nanocrystals, Nature 436 (2005) 91–94, https://doi.org/10.1038/nature03832.

[24] N. Pradhan, D. Goorskey, J. Thessing, X. Peng, An alternative of CdSe nanocrystal emitters: pure and tunable impurity emissions in ZnSe nanocrystals, J. Am. Chem. Soc. 127 (2005) 17586–17587, https://doi.org/10.1021/ja055557z.

[25] C. Wang, Z. Hu, S. Xu, Y. Wang, Z. Zhao, Z. Wang, Y. Cui, Tuning the emission of aqueous Cu: ZnSe quantum dots to yellow light window, Nanotechnology 26 (2015) 305601.

[26] A. Goudarzi, G.M. Aval, S.S. Park, M.-C. Choi, R. Sahraei, M.H. Ullah, A. Avane, C.-S. Ha, Low-temperature growth of nanocrystalline Mn-doped ZnS thin films prepared by chemical bath deposition and optical properties, Chem. Mater. 21 (2009) 2375–2385, https://doi.org/10.1021/cm803329w.

[27] S. Darafarin, R. Sahraei, A. Daneshfar, Effect of deposition temperature on structural and optical properties of chemically grown nanocrystalline Ni doped ZnS thin films, J. Alloys Compd. 658 (2016) 780–787, https://doi.org/10.1016/j.jallcom.2015.10.272.

[28] H. Khallaf, G. Chai, O. Lupan, L. Chow, S. Park, A. Schulte, Characterization of gallium-doped CdS thin films grown by chemical bath deposition, Appl. Surf. Sci. 255 (2009) 4129–4134, https://doi.org/10.1016/j.apsusc.2008.10.115.

[29] P. Roy, S.K. Srivastava, In situ deposition of Sn-doped CdS thin films by chemical bath deposition and their characterization, J. Phys. D Appl. Phys. 39 (2006) 4771, https://doi.org/10.1088/0022-3727/39/22/006.

[30] M. Muthusamy, S. Muthukumaran, M. Ashokkumar, Composition dependent optical, structural and photoluminescence behaviour of CdS:Al thin films by chemical bath deposition method, Ceram. Int. 40 (2014) 10657–10666, https://doi.org/10.1016/j.ceramint.2014.03.050.

[31] M. Makkar, R. Viswanatha, Frontier challenges in doping quantum dots: synthesis and characterization, RSC Adv. 8 (2018) 22103–22112, https://doi.org/10.1039/c8ra03530j.

[32] L. Ma, X. Ai, X. Wu, Effect of substrate and Zn doping on the structural, optical and electrical properties of CdS thin films prepared by CBD method, J. Alloys Compd. 691 (2017) 399–406, https://doi.org/10.1016/j.jallcom.2016.08.298.

[33] K.L. Silva, L. Silmi, S.L. Brock, Effect of metal ion solubility on the oxidative assembly of metal sulfide quantum dots, J. Chem. Phys. 151 (2019) 234715, https://doi.org/10.1063/1.5128932.

[34] T. Ling, S.A. Kulinich, Z.L. Zhu, S.Z. Qiao, X.W. Du, Highly conductive CdS inverse opals for photochemical solar cells, Adv. Funct. Mater. 24 (2014) 707–715, https://doi.org/10.1002/adfm.201300734.

[35] H. Li, Z. Wang, Y. He, S. Meng, Y. Xu, S. Chen, X. Fu, Rational synthesis of $Mn_xCd_{1-x}S$ for enhanced photocatalytic H_2 evolution: effects of S precursors and the feed ratio of Mn/Cd on its structure and performance, J. Colloid Interface Sci. 535 (2019) 469–480, https://doi.org/10.1016/j.jcis.2018.10.018.

[36] N. Razgoniaeva, P. Moroz, M. Yang, D.S. Budkina, H. Eckard, M. Augspurger, D. Khon, A.N. Tarnovsky, M. Zamkov, One-dimensional carrier confinement in "giant" CdS/CdSe excitonic nanoshells, J. Am. Chem. Soc. 139 (2017) 7815–7822, https://doi.org/10.1021/jacs.7b02054.

[37] K.C. Wilson, E. Manikandan, M. Basheer Ahamed, B.W. Mwakikunga, Nanocauliflower like structure of CdS thin film for solar cell photovoltaic applications: in situ tin doping by chemical bath deposition technique, J. Alloys Compd. 585 (2014) 555–560, https://doi.org/10.1016/j.jallcom.2013.09.185.

[38] F. Rodríguez-Mas, J.C. Ferrer, J.L. Alonso, D. Valiente, S.F. de Ávila, A comparative study of theoretical methods to estimate semiconductor nanoparticles' size, Crystals 10 (2020) 226, https://doi.org/10.3390/cryst10030226.
[39] B. Pejova, A. Tanuševski, I. Grozdanov, Semiconducting thin films of zinc selenide quantum dots, J. Solid State Chem. 177 (2004) 4785–4799, https://doi.org/10.1016/j.jssc.2004.06.011.
[40] F.J. Willars-Rodríguez, I.R. Chávez-Urbiola, M.A. Hernández-Landaverde, P. Vorobiev, R. Ramírez-Bon, Y.V. Vorobiev, Effects of tin-doping on cadmium sulfide (CdS:Sn) thin-films grown by light-assisted chemical bath deposition process for solar photovoltaic cell, Thin Solid Films 653 (2018) 341–349, https://doi.org/10.1016/j.tsf.2018.03.046.
[41] L. Aziz, N. Sabih, S. Mehmood, A. Ali, M.U. Hassan, A.S. Bhatti, Anomalous Arrhenius and Berthelot behavior of temperature dependent photoluminescence of Mn-doped ZnS nanostructures, Ceram. Int. 46 (2020) 9794–9801, https://doi.org/10.1016/j.ceramint.2019.12.252.
[42] J. Hou, H. Zhao, F. Huang, Q. Jing, H. Cao, Q. Wu, S. Peng, G. Cao, High performance of Mn-doped CdSe quantum dot sensitized solar cells based on the vertical ZnO nanorod arrays, J. Power Sources 325 (2016) 438–445, https://doi.org/10.1016/j.jpowsour.2016.06.070.
[43] H. Ye, H. Wang, F. Zhao, B. Zeng, A one-pot hydrothermal synthesis of graphene/CdS:Mn photocatalyst for photoelectrochemical sensing of glutathione, RSC Adv. 7 (2017) 45792, https://doi.org/10.1039/c7ra09075g.
[44] J. Yuvaloshini, R. Shanmugavadivu, Influence of Ni on structural, morphological and optical properties of nanocrystalline CdS thin films prepared by chemical bath deposition method, J. Mater. Sci. Mater. Electron. 27 (2016) 9379–9383, https://doi.org/10.1007/s10854-016-4980-9.
[45] S. Chaure, Investigation of the effect of Manganese doping in CdS nanocrystalline thin films, Mater. Res. Express 6 (2019), 025912, https://doi.org/10.1088/2053-1591/aad4e1.
[46] T. Sivaraman, V.S. Nagarethinam, A.R. Balu, K. Usharani, Structural, morphological, optical and electrical properties of CdS thin films simultaneously doped with magnesium and chlorine, J. Mater. Sci. Mater. Electron. 27 (2016) 1158–1164, https://doi.org/10.1007/s10854-015-3865-7.
[47] A.M. Smith, S. Nie, Semiconductor nanocrystals: structure, properties, and band gap engineering, Acc. Chem. Res. 43 (2010) 190–200, https://doi.org/10.1021/ar9001069. TRPL Results.